THE JOURNAL OF BIOLOGICAL CHEMISTRY Vol. 278, No. 47, Issue of November 21, pp. 46741–46749, 2003
Printed in U.S.A.

Adenosine A_{2A}-Dopamine D_2 Receptor-Receptor Heteromerization

QUALITATIVE AND QUANTITATIVE ASSESSMENT BY FLUORESCENCE AND BIOLUMINESCENCE ENERGY TRANSFER*[S]

Received for publication, June 18, 2003, and in revised form, August 20, 2003
Published, JBC Papers in Press, August 21, 2003, DOI 10.1074/jbc.M306451200

Meritxell Canals,[a,b] Daniel Marcellino,[a,b] Francesca Fanelli,[c,d] Francisco Ciruela,[a] Piero de Benedetti,[d] Steven R. Goldberg,[e] Kim Neve[j], Kjell Fuxe,[f] Luigi F. Agnati,[g] Amina S. Woods,[e] Sergi Ferré,[e] Carme Lluis,[a] Michel Bouvier,[h] and Rafael Franco[a,i]

From the [a]Department of Biochemistry and Molecular Biology of the University of Barcelona E-08028, Spain, the [c]Dulbecco Telethon Institute, the [d]Department of Chemistry, and the [g]Department of Biomedical Sciences, University of Modena and Reggio Emilia, 41100 Modena, Italy, the [e]National Institute on Drug Abuse, DHHS, NIH, Intramural Research Program, Baltimore, Maryland 21224, the [f]Department of Neuroscience, Division of Cellular and Molecular Neurochemistry, Karolinska Institutet, S-171 77 Stockholm, Sweden, the [h]Department of Biochemistry, University of Montreal, Montreal, Quebec H3C 3J7, Canada, and [j]the Department of Veterans Affairs Medical Center, Portland, Oregon 97239

There is evidence for strong functional antagonistic interactions between adenosine A_{2A} receptors (A_{2A}Rs) and dopamine D_2 receptors (D_2Rs). Although a close physical interaction between both receptors has recently been shown using co-immunoprecipitation and co-localization assays, the existence of a A_{2A}R-D_2R protein-protein interaction still had to be demonstrated in intact living cells. In the present work, fluorescence resonance energy transfer (FRET) and bioluminescence resonance energy transfer (BRET) techniques were used to confirm the occurrence of A_{2A}R-D_2R interactions in co-transfected cells. The degree of A_{2A}R-D_2R heteromerization, measured by BRET, did not vary after receptor activation with selective agonists, alone or in combination. BRET competition experiments were performed using a chimeric D_2R-D_1R in which helices 5 and 6, the third intracellular loop (I3), and the third extracellular loop (E3) of the D_2R were replaced by those of the dopamine D_1 receptor (D_1R). Although the wild type D_2R was able to decrease the BRET signal, the chimera failed to achieve any effect. This suggests that the helix 5-I3-helix 6-E3 portion of D_2R holds the site(s) for interaction with A_{2A}R. Modeling of A_{2A}R and D_2R using a modified rhodopsin template followed by molecular dynamics and docking simulations gave essentially two different possible modes of interaction between D_2R and A_{2A}R. In the most probable one, helix 5 and/or helix 6 and the N-terminal portion of I3 from D_2R approached helix 4 and the C-terminal portion of the C-tail from the A_{2A}R, respectively.

Heptaspanning membrane receptors (HSMRs)[1] or G protein-coupled receptors (GPCRs) were initially considered monomeric proteins that only interact with G proteins. However, it has become clear that HSMRs are oligomeric structures formed by receptor homodimers, heterodimers, and multimers and a variety of proteins interacting at the plane of the membrane (horizontal level) or across the plane of the membrane (vertical level) (1–6). Current investigation of these macromolecular complexes offers great potential for functional proteomics and offers deeper insight into information handling at the cellular level. The occurrence of oligomeric complexes involving GPCRs and intracellular and extracellular proteins indicates that conformational changes in response to ligand binding to a receptor may be transmitted to other protein molecules within the multimolecular complex. The conformational changes transmitted by direct protein-protein interactions constitute a first level of regulation of a receptor (6). Heteromeric complexes are not distributed randomly in the membrane and form clusters following agonist-induced activation. The intercommunication between heteromeric receptor complexes within clusters represents a second level of regulation (6). It should also be considered that the plasma membrane is not an isomorphic structure, but a structure made by patches with various chemical-physical characteristics (*e.g.* lipid rafts). Therefore, multimeric complexes and agonist-induced clusters may follow preferential routes (owing, for example, to the low viscosity of the membrane) to make contact in the membrane or may be kept as isolated multimeric complexes or clusters within a patch (6).

An example of intercommunicating receptors is that formed by adenosine A_{2A} receptors (A_{2A}Rs) and dopamine D_2 receptors (D_2Rs). Important experimental evidence has accumulated in relation to the existence of functional interactions between A_{2A}Rs and D_2Rs in the basal ganglia (5, 7, 8). These two receptors are specifically localized in one subtype of neurons,

* This work was supported by European Union Grant QLG3-CT-2001-01056; Ministerio de Ciencia y Tecnología Grants BIO1999-0601-C02-02, SAF2002-03293, and SAF2001-3474; Fundacio la Caixa Grant 02/056-00; Fundació Marató of Catalonian Telethon Grant 01/012710; Telethon-Italy Grant TCP00068 and a fellowship for European Advanced Light Microscope Facility short term program at the European Molecular Biology Laboratory in Heidelberg, Germany (to D. M.). The costs of publication of this article were defrayed in part by the payment of page charges. This article must therefore be hereby marked "*advertisement*" in accordance with 18 U.S.C. Section 1734 solely to indicate this fact.

[S] The on-line version of this article (available at http://www.jbc.org) contains Figs. 11 and 12.

[b] These authors contributed equally to this work.

[i] To whom correspondence should be addressed: Dept. of Biochemistry and Molecular Biology, University of Barcelona, Martí i Franquès 1, 08028 Barcelona, Spain. Tel.: 34-93-402-12-08; Fax: 34-93-402-12-19; E-mail: r.franco@bq.ub.es.

[1] The abbreviations used are: HSMR, heptaspanning membrane receptor; GPCR, G protein-coupled receptor; YFP, yellow fluorescent protein; BRET, bioluminescence resonance energy transfer; FRET, fluorescence resonance energy transfer; E_n, extracellular loop n; I_n, intracellular loop n; Mes, 4-morpholineethanesulfonic acid; ANOVA, analysis of variance; Rluc, *Renilla* luciferase; EYFP enhanced yellow fluorescent protein; CHO, Chinese hamster ovary; GFP, green fluorescent protein; PDB, Protein Data Bank; GABA, γ-aminobutyric acid; PBS, phosphate-buffered saline; CH, channel; A_{2A}R, adenosine A_{2A} receptor; D_nR, dopamine D_n receptor.

the striatopallidal γ-aminobutyric acid (GABA)-containing neurons, on which both receptors express their highest density in the brain. The striatopallidal GABAergic neurons play a key role in the pathophysiology of basal ganglia disorders, including Parkinson's disease, and it is a common pathway for the rewarding effects in drug abuse, as well as the antipsychotic effects of neuroleptics. Relationships between $A_{2A}R$ and D_2R have been demonstrated at the biochemical, functional, and behavioral levels, where it has been suggested that the adenosine/dopamine cross-talk in the central nervous system may provide new therapeutic approaches for Parkinson's disease, schizophrenia and drug addiction (5, 7, 8). At the biochemical level, two kinds of antagonistic $A_{2A}R$-D_2R interaction have been discovered, which can explain the $A_{2A}R$-D_2R interaction observed at both the functional and behavioral levels. In the first place, by means of their intramembrane interaction, the stimulation of $A_{2A}R$ decreases the affinity of D_2R for agonists (9). Second, the stimulation of D_2R, a $G_{i/o}$ protein-coupled receptor, inhibits cAMP accumulation induced by the stimulation of the $G_{s/olf}$ protein-coupled $A_{2A}R$ (10). The intramembrane $A_{2A}R$-D_2R interaction implies a close physical interaction between the two receptors. In fact, the pharmacology of D_2R is affected by adenosine analogs activating $A_{2A}R$. Also, co-immunoprecipitation, co-aggregation, and co-internalization of $A_{2A}R$ and D_2R have been recently reported in co-transfected cell lines (10). The existence of a heterologous, *i.e.* D_2R-mediated, desensitization of $A_{2A}R$ (10) is further evidence of the $A_{2A}R$-D_2R cross-talk. However, the demonstration of protein-protein interactions between both receptors in living cells remains to be demonstrated. In the present study, $A_{2A}R$-D_2R heterodimerization in a heterologous mammalian expression system has been investigated by both fluorescence resonance energy transfer (FRET) and bioluminescence resonance energy transfer (BRET). The influence of receptor density and agonist binding on the degree of $A_{2A}R$-D_2R heteromerization was assessed. The results indicate that the two receptors heteromerize and that changes in heteromerization do not occur in response to agonists. Based on the results of biochemical, biophysical, and computational experiments, insights have been gained into $A_{2A}R$-D_2R heterodimer interface.

EXPERIMENTAL PROCEDURES

Cell Lines—HEK-293T cells (American Type Tissue Culture, Manassas, VA) were grown in Dulbecco's modified Eagle's medium supplemented with 2 mM L-glutamine, 100 units/ml penicillin/streptomycin, and 10% (v/v) fetal bovine serum (FBS) at 37 °C and in an atmosphere of 5% CO_2. Cells were passaged when they were 80–90% confluent. All cell culture reagents were from Invitrogen.

Expression Vectors—The human cDNA for Flag-$A_{2A}R$ without its stop codon was amplified using sense and antisense primers harboring unique EcoRI and BamHI sites. The fragment then was subcloned to be in-frame with either *Rluc* or EYFP into the EcoRI and BamHI restriction site of a *Renilla* luciferase-expressing vector (pcDNA3.1-Rluc) or the enhanced yellow variant of GFP (pEYFP-N1; Clontech, Heidelberg, Germany), respectively, to give the two plasmids, $pA_{2A}R$-Rluc and $pA_{2A}R$-EYFP, that express *Rluc* or EYFP on the C-terminal ends of the receptor. The human $D_{2L}R$ was also cloned in the pGFP2-N3(h) and pEYFP-N1 vectors in a similar fashion, however, subcloned into the EcoRI and KpnI site of each respective vector to be in-frame with the GFP fluorescent protein variants, GFP2 and EYFP, respectively. The previously characterized chimeric D_2R-D_1R, in which helices 5 and 6 and third intracellular (I3) and third extracellular (E3) loops of the D_2R have been swapped by the corresponding sequence from the D_1R, was described previously (11). The positive control vector used for the FRET experiments, pGFP2-EYFP, was a gift from the laboratory of R. Pepperkok (EMBL, Heidelberg, Germany) (described in Ref. 12).

Transient Transfections—HEK-293T cells growing on coverslips in 6-well dishes were transiently transfected with 10 μg of DNA encoding the indicated proteins by calcium phosphate precipitation (13). For FRET experiments the LipofectAMINE transfection reagent, FuGENE 6™ (Roche Molecular Biochemicals), was utilized following the product protocol. In both cases and to maintain the ratio of DNA in co-transfections, the empty vector, pcDNA3.1, was used to equilibrate the amount of total DNA transfected. 24 h after transfection, the medium was replaced and cells were then cultured in the same medium until harvested 32, 48, or 72 h after transfection. For FRET experiments cells were fixed with a 3.5% paraformaldehyde solution in PBS for 15 min at room temperature, before washing in PBS and mounting onto slides.

cAMP Determination—The accumulation of cAMP was measured by a [^{3}H]cAMP assay system (Amersham Biosciences) as described in the manual from the manufacturer. Transfected HEK-293 cells (2×10^6 cells/sample) were serum-starved, preincubated with 50 mM Ro 20-1724, a phosphodiesterase inhibitor (Calbiochem, St. Diego, CA) for 10 min, and then stimulated with the indicated concentrations of agonists, CGS21680 ($A_{2A}R$), quinpirole (D_2R), and forskolin (all from Sigma), for 15 min prior to the determination of cAMP levels.

FRET-based Acceptor Photo-bleaching Experiments Analyzed by Confocal Microscopy—Transiently transfected HEK-293T cells were plated onto 15-mm glass coverslips and mounted onto slides using Mowiol mounting medium. Confocal laser scanning microscopy was performed using a Leica SP2 microscope (Leica Microsystems, Mannheim, Germany) equipped with an acousto-optical beamsplitter, a 100-milliwatt argon laser for excitation at 514 nm, and a 20-milliwatt blue diode laser for excitation at 405 nm. GFP2 was excited with the 405 nm laser, YFP was excited with the 514 nm laser, and images were acquired in the following sequence. (i) A pre-photo-bleach YFP (acceptor) image was acquired by scanning while exciting with the 514 nm laser line. (ii) A pre-photo-bleach GFP2 (donor) image was acquired by scanning while exciting with 405 nm laser line. (iii) A region of interest was selected and the acceptor (YFP) was subsequently photo-bleached by scanning repeatedly with the 514 nm laser line until fluorescence signals were at background levels. (iv) A post-photo-bleach image for GFP2 was acquired by scanning with the 405 nm laser line. (v) a second post-photo-bleach image for EYFP was acquired by scanning with the 514 nm laser. In all cases, the spectral imaging was obtained at three fluorescence detection channels (Ch) set to the following ranges: Ch 1: 490–510 nm, Ch 2: 520–540 nm, Ch 3: 545–565 nm. Settings for gain and offset of the detectors were identical for all experiments to keep the relative contribution of the fluorophores to the detection channels constant for spectral un-mixing (see below). The contributions of the GFP variants, GFP2 and YFP, to each of the three detection channels (spectral signature) were measured in experiments with cells expressing only one of these proteins and normalized to the sum of the signal obtained in the three detection channels

FRET Experiments Analyzed by Fluorimetry—Forty-eight hours after transfection, cells were rapidly washed twice in PBS, detached, and resuspended in the same buffer. To control the number of cells, the protein concentration of the samples was determined using a Bradford assay kit (Bio-Rad) using bovine serum albumin dilutions as standards. Cell suspension (20 μg of protein) was distributed in duplicate into 96-well microplates (black plates with a transparent bottom). Plates were read in a Fluostar Optima Fluorimeter (BMG Labtechnologies, Offenburg, Germany) equipped with a high energy xenon flash lamp, using a 10-nm bandwidth excitation filter at 400 nm (393–403 nm), and 10-nm bandwidth emission filters corresponding to 506–515 nm filter (Ch 1) and 527–536 nm filter (Ch 2). Gain settings were identical for all experiments to keep the relative contribution of the fluorophores to the detection channels constant for spectral un-mixing. The contributions of the GFP variants, GFP2 and YFP proteins alone, to the two detection channels (spectral signature) were measured in experiments with cells expressing only one of these proteins and normalized to the sum of the signal obtained in the two detection channels. The spectral signatures of the different receptors fused to either GFP2 or YFP did not significantly vary from the determined spectral signatures of the fluorescent proteins alone.

Quantitation of FRET—Linear un-mixing was done as described by Zimmermann *et al.* (12) to separate the two emission spectra. To determine the fluorescence emitted by each of two individual fluorophores (FluoA corresponding to the donor and FluoB corresponding to the acceptor) in FRET experiments analyzed by confocal microscopy, the following formula was applied for every image pixel i,

$$\mathrm{FluoA}(i) = \frac{S(i)}{1 + \frac{1}{R(i)}} \quad \text{and} \quad \mathrm{FluoB}(i) = \frac{S(i)}{1 + R(i)} \qquad \text{(Eq. 1)}$$

where

$$S(i) = \sum_{k=1}^{n} Ch_k(i) \quad \text{(Eq. 2)}$$

$$R(i) = \frac{\text{FluoA}(i)}{\text{FluoB}(i)} = \frac{B_y Q(i) - B_x}{A_x - A_y Q(i)} \quad \text{(Eq. 3)}$$

and

$$Q(i) = \frac{Ch_x(i)}{Ch_y(i)} \quad \text{(Eq. 4)}$$

where Ch_x and Ch_y represent the signals in detection channels x and y, and A_x, B_x and A_y, B_y represent the normalized contributions of FluoA or FluoB to channels x and y, as they are known from the spectral signatures of the fluorescent proteins. For the fluorimetric experiments, the same equations were applied. By these equations the fluorophore signals, FluoA and FluoB, were calculated using the processing routines written (and generously provided) by T. Zimmermann (EMBL, Heidelberg, Germany) in Interactive Data Language (IDL, Research Systems Inc., Boulder, CO).

According to Zimmermann *et al.* (12), apparent FRET efficiencies E_A in acceptor photo-bleaching experiments were calculated for each pixel i according to Equation 5.

$$E_A(i) = 1 - \frac{F^D(i)}{F^D_{pb}(i)} \quad \text{(Eq. 5)}$$

F^D represents the emitted donor fluorescence (FluoA) before and F^D_{pb} after photo-bleaching of the acceptor. For the fluorimetric experiments, FRET efficiency was calculated as direct sensitization of the acceptor corresponding to acceptor fluorescence (FluoB) after excitation at 400 nm.

BRET Experiments—Forty-eight hours after transfection, cells were rapidly washed twice in PBS, detached, and resuspended in the same buffer. To control the number of cells, sample protein concentration was determined using a Bradford assay kit (Bio-Rad, Munich, Germany) using bovine serum albumin dilutions as standards. To quantify A_{2A}R-*Rluc* and D2-YFP expression, cell suspension (20 μg of protein) was distributed in duplicate into 96-well microplates (Corning 3604, white plates with transparent bottom). The fluorescence was measured using a Packard FluoroCount™ with an excitation filter of 485 nm and an emission filter of 530 nm using the following parameters: gain of 1, photomultiplier fixed at 1100 V, and read time of 1 s. Fluorescence was quantified as in-fold over the background (mock-transfected cells). The same samples were incubated for 10 min with 5 μM coelenterazine H (Molecular Probes, Eugene, OR), and the luminescence was measured using a Packard LumiCount™ with the following parameters: gain of 1, photomultiplier fixed at 700 V, and a read time of 1 s. For BRET measurement, 20 μg of cell suspension were distributed in duplicates in 96-well microplates (Corning 3600, white opaque plates) and 5 μM coelenterazine H was added. After 1 min the readings were collected using a Fusion microplate analyzer (Packard, Meriden, CT) that allows the integration of the signals detected in the 440–500- and the 510–590-nm windows using filters with the appropriate band pass. The BRET ratio is defined as [(emission at 510–590)/(emission at 440–500)] − *Cf* where *Cf* corresponds to (emission at 510–590)/(emission at 440–500) for the -*Rluc* construct expressed alone in the same experiment.

Subcellular Membrane Isolation—HEK-293T cells transiently co-transfected with the A_{2A}R-*Rluc* and D_2RYFP were grown in 100-mm dishes to 80–90% confluence. Cells were washed twice with ice-cold PBS and lysed with 2 ml of ice-cold hypotonic lysis buffer (20 mM HEPES, pH 7.4, 2 mM EDTA, 2 mM EGTA, 6 mM $MgCl_2$, 1 mM phenylmethylsulfonyl fluoride, and 1:100 dilution of a protease inhibitor mixture). Lysate was then sonicated for 30 s, (3 strokes with 1-min delay between strokes) followed by two 10-s bursts in a Polytron tissue grinder. Cellular debris and unlysed cells were removed by centrifuging at 1500 rpm for 5 min at 4 °C. Sucrose was added to achieve a final concentration of 0.2 M, and 2 ml were applied to the top of a discontinuous step gradient (5 ml/step) made at 0.5, 0.9, 1.2, 1.35, 1.5, and 2.0 M sucrose in lysis buffer. The samples were then centrifuged for 16 h at 27,000 rpm at 4 °C in a Beckman SW28 rotor. The plasma membrane was recovered in the sucrose gradient at the interface between 0.5 and 0.9 M. The endoplasmic reticular membrane samples were recovered at the interface between 1.35 and 1.5 M, and luminescence was detected. For the verification of isolated membranes as either plasma or endoplasmic reticulum membranes, fractions were then precipitated with cold acetone overnight and analyzed by Western blotting using monoclonal antibodies against Na^+K^+-ATPase pump (1:250 dilution, Sigma) and calnexin (1:500 dilution, BD Transduction Laboratories).

Raft Disruption—HEK-293T cells were serum-starved overnight 24 h after transfection. Cholesterol depletion was achieved by incubation for 1 h at 37 °C with 2% 2-hydroxypropyl-β-cyclodextrin (β-CD, Sigma) in Dulbecco's modified Eagle's medium. Cholesterol repletion was done, after washing twice with fresh medium, by incubation for 1 h at 37 °C with 0.4% β-CD and 16 mg/ml cholesterol (Sigma). Complete raft disruption was assessed as caveolin-1 displacement in a discontinuous sucrose gradient. For this, confluent control or depleted cells were washed twice with ice-cold PBS, scraped, and resuspended into 2 ml of 500 mM Na_2CO_3, pH 11.0. Cells were sequentially homogenized using a Polytron (3 times, 10 s), a syringe (20 times) and a sonicator (3 times, 30 s), placed at the bottom of an ultracentrifuge tube and adjusted to 45% sucrose in Mes-buffered saline (25 mM Mes, 0,15 M NaCl, pH 6.5). A discontinuous 5–35% sucrose gradient was formed above in Mes-buffered saline containing 250 mM Na_2CO_3, pH 6.5. After centrifugation at 105,000 × *g* for 18 h at 4 °C in a SW41.Ti rotor (Beckman), fractions were collected and analyzed by Western blot using an antibody against caveolin-1 (BD Transduction Laboratories, Lexington, KY). β-CD effects were also tested by mitogen-activated protein kinase phosphorylation analysis; treated cells were directly resuspended in loading buffer and analyzed by Western blot using the antibodies against phosphorylated or total extracellular signal-regulated kinase-1/2 (Sigma).

Three-dimensional Model Building of the Human D_2R and Human A_{2A}R—For the D_2R, the whole sequence of the human short variance (SWISS-PROT entry P14416) was modeled. The intracellular loops 1, 2, and 3 and the extracellular loops 1, 2, and 3 will be, respectively, abbreviated as I1, I2, I3, E1, E2, and E3. Building of I3 (sequence 215–334) was carried out by comparative modeling (by means of MODELER; Ref. 14) by using the domain A2 of Glycyl-TRNA synthetase (PDB entry 1ati; sequence 393–505) as a template, according to the results of fold recognition by means of THREADER (15). This template, characterized by a three-layer ($\alpha\beta\alpha$) sandwich architecture and a Rossmann fold, resulted to be the top hit, holding a reliable *z*-score (*i.e.* 3.65). Indeed, secondary structure predictions made by four different methods agree acceptably well with the secondary structures computed on the I3 in the selected average minimized structure of D_2R. Similarly, E2 was separately obtained by Molecular Dynamics simulations. A chimeric rhodopsin template (PDB entry 1F88; Ref. 16) was built by introducing the E2 and I3 models after deleting the rhodopsin segments 176–201, 229–235, and 240–243. This template was employed to generate 25 different models of the D_2R according to the sequence alignment shown in Fig. 11 (available as supplementary material in the on-line version of this article). Among these models, the one showing the lowest degree of violation of the structural restraints was used to generate the input structures for Molecular Dynamics simulations. Automatic rotation of the side chains when in bad conformation was performed, leading to different input arrangements. These arrangements were subjected to energy minimization and 150-ps runs of Molecular Dynamics simulations, by means of the program CHARMM (17). Minimizations were carried out by using 1500 steps of steepest descent followed by a conjugate gradient minimization, until the root mean square gradient was less than 0.001 kcal/mol Å. A distance dependent dielectric term ($\epsilon = 4r$) was chosen. The "united atom approximation" was used. The systems were heated to 300 K with 5-K rise, every 100 steps per 6000 steps, by randomly assigning velocities from the Gaussian distribution. After heating, the system was allowed to equilibrate for 34 ps. The lengths of the bonds involving the hydrogen atoms were constrained according to the SHAKE algorithm, allowing an integration time step of 0.001 ps. A disulfide bridge was imposed to form between Cys-107 (3.25) (in parentheses, the numbering from Ballesteros and Weinstein (Ref. 18) for the amino acids in the helix-bundle is reported) and Cys-182 in E2. The secondary structure of the seven helix-bundle was preserved by using the nuclear Overhauser effect constraints. These constraints were applied between the backbone oxygen atoms of residue i and the backbone nitrogen atom of residue $i + 4$, excluding prolines. Different combinations of intra-helix distance constraints were also probed. The non-canonical α-helical structure in the extracellular half of helix 7 was preserved by nuclear Overhauser effect constraints. The structures averaged over the 200 structures collected during the last 100 ps of the equilibrated trajectories and minimized were comparatively analyzed. One of the average arrangements obtained was then considered for docking simulations.

Also for the human A_{2A}R, the whole sequence was modeled (SWISS-PROT entry P29274). Building of the C-tail (*i.e.* the 303–412 segment) was primarily achieved by comparative modeling (14). Two different models of this receptor portion were achieved: (*a*) **model 1**, obtained by

using the domain A3 of transketolase (PDB entry 1trk; sequence 544–680) as a template and (*b*) **model 2**, obtained by using the domain 2 of the cytidine deaminase (PDB entry 1ctt; sequence 180–294) as a template, according to the results of fold recognition (15). Indeed, both 1trkA3 and 1ctt02 domains, which share a three-layer ($\alpha\beta\alpha$) sandwich architecture, were the top hits of the THREADER run, characterized by comparable *z*-scores (*i.e.* 3.17 and 3.14, respectively). The agreement between the secondary structures predicted on the $A_{2A}R$ C-tail sequence and that computed on the C-tail models in the average minimized structures of the receptor is acceptable, especially for the C-tail based upon 1ctt02. Three modified rhodopsin templates (PDB entry 1F88; Ref. 16) were built in which the segments 227–235, 240–246, and 321–348 were deleted and either **model 1** or **model 2** of the C-tail from the human $A_{2A}R$ sequence was added. In particular, one template holds "model 1 C-tail," whereas the other two templates hold "model 2 C-tail," but in a slightly different orientation. Each of these templates was used to generate 50 models according to alignment reported in Fig. 12 (available as supplementary material in the on-line version of this article). α-Helical restraints were applied to the amino acid stretches 198–209, 221–228, 224–227, and 299–306. The best $A_{2A}R$ models obtained from each of the three MODELLER runs were subjected to refinement of I3 by means of MODELLER, leading to other three sets of structures. From each of these three sets of structures, one model was finally selected and subjected to automatic rotation of the side chains when in bad conformation, leading to different input arrangements. For the $A_{2A}R$ model holding the "**model 1**" C-tail and for that holding the "**model 2**" C-tail, 19 and 17 different input structures were, respectively, subjected to energy minimization and Molecular Dynamics simulations. The same computational protocol as that employed for the D_2R was followed. A disulfide bridge was imposed to form between Cys-77 (3.25) and Cys-159 in E2. The structures averaged over the 200 structures collected during the last 100 ps of the equilibrated trajectories and minimized were then analyzed. Eleven average arrangements were finally considered for docking simulations.

Computations: Rigid Body Docking Simulations—One selected average arrangement for the human D_2R was subjected to rigid body docking simulations with 11 different average arrangements of the human $A_{2A}R$. Docking simulations were carried out by means of two different rigid body docking programs, ZDOCK 2.1 (19) and ESCHER (20). Default conditions were used. Each ZDOCK run provided 2000 solutions filtered according to the shape complementarity score. On the other hand, each ESCHER run produced 30,000 solutions that were then filtered according to both shape and electrostatic complementarity, by using bump and charge cutoffs of 200 and −200, respectively. The filtered ZDOCK and ESCHER solutions were then subjected to a filter made in-house that discharged all the solutions that violated the membrane topology requirements. A few selected D_2R-$A_{2A}R$ complexes, representatives of the most populated docking solutions, were then subjected to manual relief of the steric conflicts followed by energy minimization.

RESULTS

Functionality of Modified $A_{2A}Rs$ and D_2Rs—The formation of $A_{2A}R$-D_2R heterodimers was demonstrated by BRET and FRET techniques in cells transfected with fusion proteins consisting of each receptor and either a fluorescent protein (GFP2, YFP) or *Renilla* luciferase (*Rluc*). Expression of fusion proteins and or the chimeric D_2R-D_1R protein was assessed by Western blot and immunocytochemistry (data not shown). The functionality of the receptor-*Rluc*, -GFP2, or -YFP constructs was assessed by the determination of cAMP levels produced in transfected cells in response to ligand binding. According to the positive coupling of $A_{2A}R$ to the adenylyl cyclase, the $A_{2A}R$ agonist CGS21680 properly induced cAMP accumulation in cells transfected with $A_{2A}R$-YFP or $A_{2A}R$-*Rluc* (Fig. 1*A*). On the other hand, in agreement with the inhibitory role of D_2R on adenylyl cyclase activity, the D_2R agonist quinpirole was able to reduce forskolin-induced cAMP levels in cells transfected with either D_2R-YFP or D_2R-GFP2 (Fig. 1*B*).

FRET Experiments—FRET and BRET approaches have been used in several studies to assess GPCR homo- and heterodimerization as reviewed by Angers *et al.* (21). By using the FRET approach with the D_2R-GFP2 and $A_{2A}R$-YFP pair, it was possible to confirm the heteromerization between $A_{2A}R$ and D_2R and to estimate the distance between the fluorophores. Using the acceptor photobleaching technique and confocal microscopy on cells expressing both receptors in the plasma membrane, a direct interaction was demonstrated between $A_{2A}R$ and D_2R (Fig. 2). FRET efficiency was determined to be in the range of 23–25%. Similar FRET efficiencies were obtained using a fluorescence plate reader as described under "Experimental Procedures" (Fig. 3). The low FRET efficiency of a negative control constituted by the pair D_2R-GFP2 and CD4-YFP demonstrated the specificity in the energy transfer between D_2R-GFP2 and $A_{2A}R$-YFP (Fig. 3). Using the theoretical curve of FRET efficiency correlated to the distance between the donor and acceptor fluorophores while assuming only a dimeric interaction, an efficiency in the range of 23–25%, indicates that the distance between fluorophores (GFP2 and YFP), both located at the C terminus of either $A_{2A}R$ or D_2R, is ~6–6.5 nm (Fig. 4).

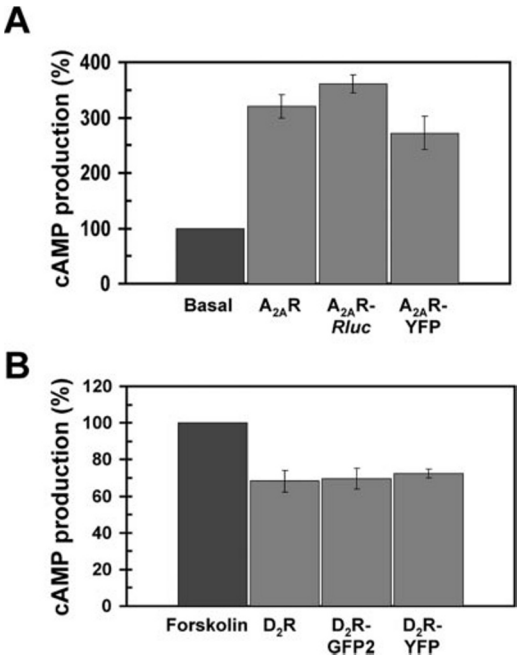

FIG. 1. **Functionality test of receptors fused to GFP variants or *Renilla* luciferase (*Rluc*).** HEK-293T cells transiently transfected with the corresponding constructs were stimulated with either 200 nM CGS21680 for $A_{2A}R$ (*panel A*), or 10 μM quinpirole in the presence of 10 μM forskolin for D_2R (*panel B*). $A_{2A}R$ induction of cAMP production is presented as percentage over basal levels (100%). As D_2R inhibits the production of cAMP, results are presented as its ability to inhibit forskolin induced cAMP production (100%). Results are a mean ± S.D. of four independent experiments performed in triplicate. One-way ANOVA showed a significant increase of cAMP production with CGS 21680 with wild-type $A_{2A}R$ and the $A_{2A}R$ fused to *Rluc* or YFP. Similarly, one-way ANOVA showed a significant decrease in forskolin-induced cAMP production with quinpirole with wild-type D_2R and the D_2R fused to GFP2 or YFP (*post hoc* Newman-Keuls test; $p < 0.05$ in all cases).

BRET Experiments—In BRET experiments, little attention has been paid to the ratio of donor to acceptor molecules; thus, the interpretation of the data has remained rather qualitative. Indeed, the level of energy transfer detected for a given concentration of donor should increase with higher concentrations of acceptor until all of the donor molecules are bound to an acceptor molecule. This follows the theory that the energy transfer will reach a plateau therefore giving rise to a saturation curve. The maximum level reached will be a function of the total number of dimers formed and of the distance between the donor and acceptor while considering the relative orientation of the proteins within the dimers. The concentration of acceptor, giving 50% of the maximum energy transfer ($BRET_{50}$), will

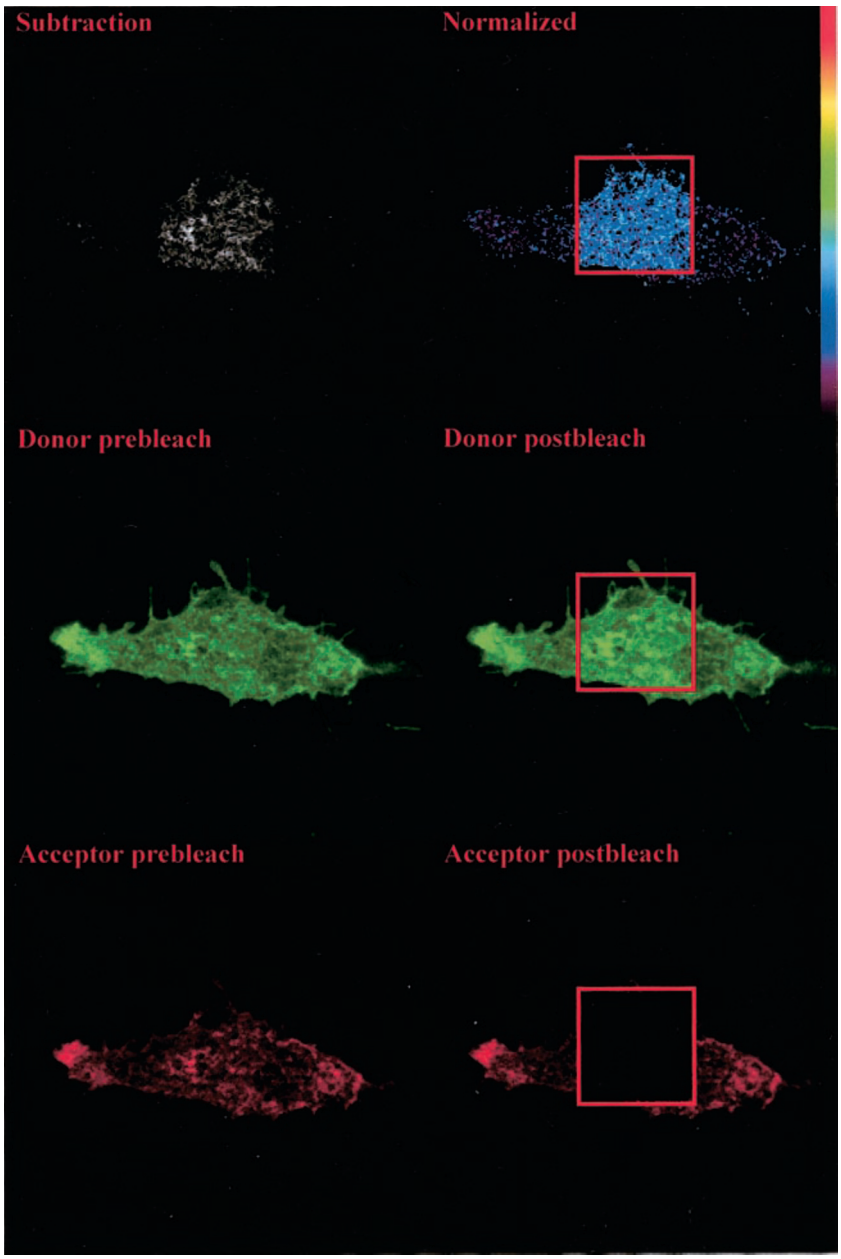

FIG. 2. **Imaging FRET efficiency of the D_2R-GFP2 and A_{2A}R-YFP pair by acceptor photo-bleaching.** HEK-293T cells were transiently transfected with the plasmid DNA for the D_2R-GFP2 and A_{2A}R-YFP constructs using a ratio of donor to acceptor DNA of 1:2 and fixed 48 h after transfection. Central panels are images of the D_2R-GFP2 donor before (*Donor prebleach*) and after (*Donor postbleach*) photo-bleaching of the A_{2A}R-YFP acceptor obtained in a central region of the lowest plane of the cell by spectral imaging and subsequent liner un-mixing as described under "Experimental Procedures." The extent of the photo-bleaching is shown in the *bottom panels* as a lack of acceptor fluorescence in the selected region after photo-bleaching (*Acceptor postbleach*) with respect to the image of the acceptor before photo-bleaching (*Acceptor prebleach*). The *top panels* represent donor un-quenching following acceptor photo-bleaching as donor postbleach − donor prebleach (subtraction) and a color representation of the FRET efficiency (normalized) calculated as indicated under "Experimental Procedures" and normalized to a scale from 0 to 1.

reflect the relative affinity of an acceptor and a donor to dimerize (22).

Here, we applied this theoretical framework to study A_{2A}R and D_2R heteromerization by constructing a BRET saturation curve in cells co-transfected with a constant amount of the A_{2A}R-*Rluc* construct while increasing concentrations of the D_2R-YFP plasmid. A positive BRET signal for the transfer of energy between A_{2A}R-*Rluc* and D_2R-YFP was obtained (Fig. 5). The BRET signal increased as a hyperbolic function of the concentration of the YFP-fusion construct added (assessed by the fluorescence emitted upon direct excitation at 480 nm) reaching an asymptote. As the pair A_{2A}R-*Rluc* and $GABA_BR2$-YFP led to an undetectable BRET signal (Fig. 5), the hyperbolic BRET signal found for the A_{2A}R-*Rluc*-D_2R-YFP indicates that the interaction between A_{2A}R and D_2R is specific.

Energy transfer between closely located receptor molecules can occur even in the absence of direct interaction (23). In fact, receptors located within specific plasma membrane microdomains, such as membrane rafts, may give rise to FRET or BRET signals not caused by real heteromerization. Raft localization of overexpressed membrane fluorescent proteins could allow a close enough proximity (<10 nm) to permit the transfer of energy. To explore this possibility, membrane rafts were disrupted by cyclodextrin treatment, and BRET assays were performed in these cells. As indicated in Fig. 3*A*, cyclodextrin did not lead to any change in the BRET signal for A_{2A}R-*Rluc*-D_2R-YFP. In addition, no change in the BRET signal was noted when cells were repleted with cholesterol after cyclodextrin treatment (Fig. 6*A*). The efficacy of the treatment was assessed by cyclodextrin-mediated extracellular signal-regulated kinase-1/2 phosphorylation, as indicated by Furuchi and Anderson (24). Raft disruption was also assessed by the redistribution of caveolin-1 from raft-enriched light fractions to heavier fractions after sucrose gradient separation (Fig. 6*B*). Taken together, this indicates that the energy transfer between A_{2A}R-*Rluc* and D_2R-YFP is the result of the formation of true heterodimers.

Stimulation with the A_{2A}R agonist CGS21680 or the D_2R agonist quinpirole, individually or in combination, did not promote any consistent change in either maximal BRET (data not shown) or $BRET_{50}$ (Fig. 7). An analysis of the subcellular distribution of the fusion proteins indicated that the lack of ago-

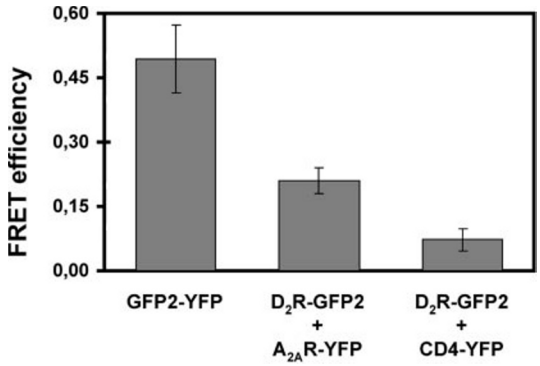

FIG. 3. **FRET efficiency of the D_2R-GFP2 and A_{2A}R-YFP pair by sensitized emission in living cells.** HEK-293T cells were transiently transfected with the plasmid DNA corresponding to D_2R-GFP2 (donor) and A_{2A}R-YFP (acceptor) proteins using a ratio of donor to acceptor DNA of 1:2, or with the positive control plasmid GFP2-YFP. Fluorescence readings were performed 48 h after transfection as described under "Experimental Procedures." Linear un-mixing of the emission signals was applied to the data (see "Experimental Procedures"), and the results are shown as the sensitized emission of the acceptor when the cells were excited at 400 nm. CD4-YFP was used as a negative control. Data are the mean ± S.D. of five independent experiments performed in duplicate. One-way ANOVA followed by Newman-Keuls test shows significant differences between GFP2-YF2 and D_2R-GFP2+A_{2A}R-YFP and between D_2R-GFP2+A_{2A}R-YFP and D_2R-GFP2+CD4-YFP ($p < 0.01$ in all cases).

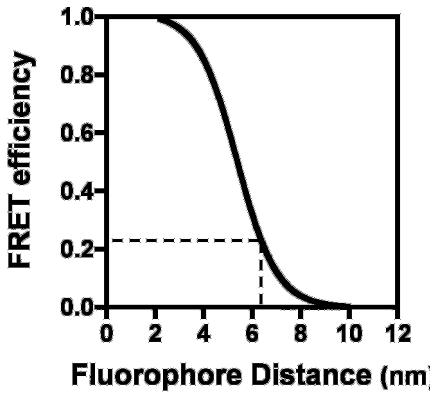

FIG. 4. **FRET efficiencies related to the distance between the fluorescent proteins.** FRET efficiencies of the GFP2 and YFP pair derived from their spectral properties were plotted as a function of the distance between the fluorescent proteins as described by Zimmermann *et al.* (12). *Dotted lines* show the relation between the determined FRET efficiency for the D_2R-GFP2-A_{2A}R-YFP pair and the approximate distance between the fluorescent proteins in this pair.

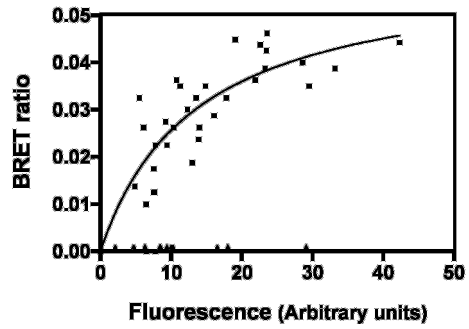

FIG. 5. **BRET saturation curve.** BRET was measured in HEK-293T cells co-expressing A_{2A}R-*Rluc* and D_2R-YFP (*squares*) or A_{2A}R-*Rluc* and $GABA_B$R2-YFP (*triangles*) constructs. Co-transfections were performed with increasing amounts of plasmid DNA for the YFP construct whereas the DNA for the *Rluc* construct was maintained constant. Both fluorescence and luminescence of each sample were measured prior to every experiment to confirm equal expression of *Rluc* while monitoring the increase of YFP expression.

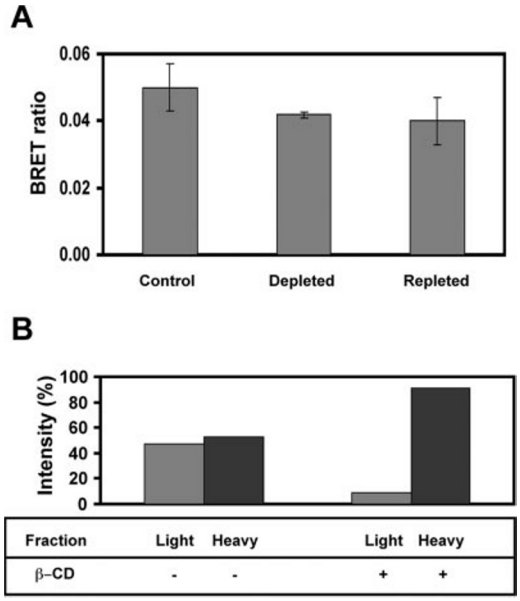

FIG. 6. ***β*-CD treatment.** BRET experiments were performed in HEK-293T cells co-transfected with the amount of plasmid DNA for the A_{2A}R-*Rluc* and D_2R-YFP constructs to give $BRET_{50}$. Cells were not treated (*Control*) or treated with 2% β-CD for 1 h (*Depleted*). Cholesterol repletion was achieved by incubating depleted cells for 1 h with 0.4% β-CD and 16 mg/ml cholesterol (*Repleted*). No differences in BRET were observed after depletion or repletion treatment (*panel A*) (analyzed with one-way ANOVA). For immunoblotting of caveolin-1 in cells treated with β-CD (*panel B*), extracts from control and treated cells were fractionated by a discontinuous sucrose gradient to obtain the light and heavy membrane fractions. Caveolin-1 was detected by Western blot in both membrane fractions. Densitometry of the bands was performed, and results are expressed as the percentage of the total intensity.

nist modulation of the BRET signal occurred in cells expressing A_{2A}-*Rluc* and D_2R-YFP in the plasma membrane (Fig. 8). These results indicate that receptor activation does not affect their oligomerization state and that the heteromers are, most probably, constitutively pre-formed. However, one cannot exclude the possibility that agonist stimulation may promote assembly/disassembly cycles that do not affect the steady-state proportion of receptors engaged in dimers.

To gain some insight into the putative heterodimer interface, a chimeric D_2R-D_1R in which helices 5, 6, I3, and E3 of the D_2R have been swapped by the corresponding sequence from the D_1R (11) was used as a competitor in BRET experiments. Although the wild-type D_2R was able to decrease the BRET signal between A_{2A}R-*Rluc* and D_2R-YFP, the D_2R-D_1R chimeric receptor failed to decrease the BRET signal even at high amounts of competitor cDNA (Fig. 9). These results are in agreement with previous studies, where we have shown that A_{2A}R does not modulate the agonist binding characteristics of this chimeric D_2R-D_1R (25). This suggests somewhere in the region of the D_2R containing helices 5, 6, I3, and E3 of the D_2R lies a critical site necessary for the heteromerization with A_{2A}R.

Computational Experiments—Further insight into the D_2R-A_{2A}R heterodimer interface was obtained by docking simulations on theoretical models of D_2R and A_{2A}R. The whole sequences of both receptors were modeled, because dimerization and/or oligomerization might also involve the cytosolic and/or the extracellular domains as recently suggested for rhodopsin (26). We are aware that structural errors might reside particularly in these receptor portions. Additionally, for this reason, we have used nine different average minimized structures of the A_{2A}R, differing in the conformations of the intracellular and extracellular domains as well as in the topology of the huge

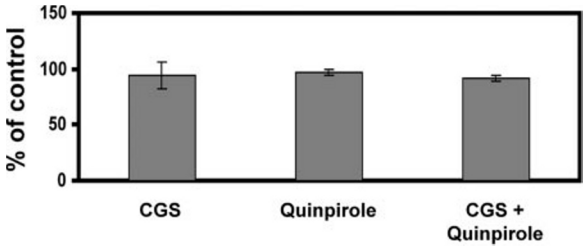

FIG. 7. **Effect of ligands on A_{2A}R-D_2R dimerization.** BRET measurements were performed after 1 h of treatment with 200 nM A_{2A}R agonist CGS21680 (*CGS*), 10 μM D_2R agonist quinpirole, or both ligands simultaneously in HEK-293T cells co-transfected with the A_{2A}R-*Rluc*-D_2R-YFP pair at the $BRET_{50}$ ratio. Data are mean ± S.D. of three independent experiments. Results are expressed as the percentage of the $BRET_{50}$ value of untreated (control) cells. No significant differences were observed between the three different groups (one-way ANOVA).

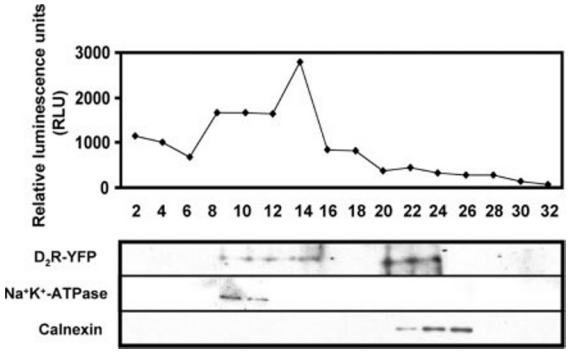

FIG. 8. **Subcellular distribution of A_{2A}R-*Rluc* and D_2R-YFP constructs.** Lysates of co-transfected HEK-293T cells as described in Fig. 7 were applied and separated on a discontinuous sucrose gradient. Fractions were subsequently analyzed for luminescence (*top panel*) and by immunoblotting (*bottom panel*). As a result of high levels of fluorescence in fractions with large concentrations of sucrose, the distribution of D_2R-YFP was analyzed by Western blot with an anti-GFP antibody. Fractions rich in plasma membrane and ER were detected by Western blot using either Na^+K^+-ATPase or calnexin antibodies, respectively.

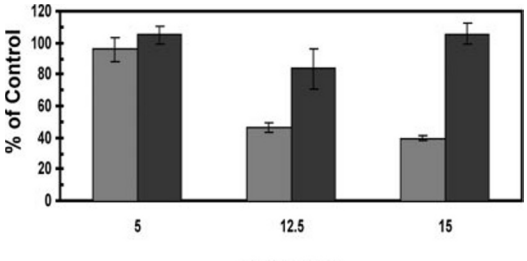

FIG. 9. **BRET competition.** HEK-293T cells were transfected with the appropriate amount of plasmid DNA for the A_{2A}R-*Rluc* and D_2R-YFP constructs corresponding to the previously determined $BRET_{50}$ (control) and with increasing amounts of D_2R cDNA (*gray bars*) or the cDNA of the dopamine D_2R-D_1R chimera (*black bars*). The BRET ratio was determined and values are expressed as a percentage of the control. Data are the mean ± S.D. of five experiments in duplicate. One-way ANOVA (with post-hoc Newman-Keuls comparisons) shows significant BRET competition with 12.5 and 15 μg of D_2R cDNA ($p < 0.001$ in both cases) and no significant differences with 12.5 or 15 μg of D_2R-D_1R cDNA.

C-tail, to probe the effect of such structural differences on the results of docking simulations. The A_{2A}R structures include four structures holding the "**model 1** C-tail" (see "Experimental Procedures") and seven structures holding the "**model 2** C-tail." Each of these structures has been docked with the selected average minimized structure of D_2R. Two different rigid-body docking programs, ZDOCK (19) and ESCHER (20), were employed. A total amount of 32,000 and 9400 filtered solutions (see "Experimental Procedures") was obtained by means of different runs of ZDOCK 2.1 and ESCHER, respectively. These solutions were subjected to an additional filter that discharged those arrangements that significantly violate the membrane topology requirements. In the majority of the more realistic (*i.e.* dimers with lower interacting enthalpy) docking solutions, the D_2R portions that participate in the heterodimer interface include the C-terminal half of helix 5, the N-terminal portion of I3 that contains a solvent-exposed stretch of positively charged amino acids (*i.e.* 217–220), helix 6, helix 7, and the segment that corresponds to helix 8 of rhodopsin (16). Among these solutions, a highly populated one (population 1, Fig. 10) is characterized by the following contacts: (*a*) **helix 5**(D_2R)-**helix 4**(A_{2A}R) and **I3$_{N\text{-term}}$**(D_2R)-**C-tail$_{C\text{-term}}$**-(A_{2A}R) and (*b*) **helix 5$_{C\text{-term}}$**(D_2R)-**helix 3$_{C\text{-term}}$**(A_{2A}R), **helix 6**(D_2R)-**helix 4**(A_{2A}R) and **I3$_{N\text{-term}}$**(D_2R)-**C-tail$_{C\text{-term}}$**(A_{2A}R); **helix 7**(D_2R) may also participate together with helix 6 in the contacts with **helix 4**(A_{2A}R). To estimate the putative interfluorophore distances in selected members of population 1, the structures of GFP and YFP (PDB entries 2emn and 1huy, respectively), have been approached to D_2R and A_{2A}R, respectively, in selected dimmers, the first amino acid of the fluorescent proteins being close to the last amino acid of the receptors. The distance between the C1 atoms of the GFP and YFP chromophores in the different complexes ranges between 6 and 8 nm, very similar to that deduced from FRET experiments.

In a less populated solution (population 2, Fig. 10), almost two different sets of contacts characterize the D_2R-A_{2A}R dimers. The first set of contacts includes: (*a*) **I2**(D_2R)-**I2**(A_{2A}R), (*b*) **helix 4$_{C\text{-teminal half}}$**(D_2R)-**helix 3$_{C\text{-terminal half}}$**($A_{2A}$R), (*c*) **helix 4$_{N\text{-terminal half}}$**($D_2$R)-**helix 5$_{N\text{-terminal half}}$**($A_{2A}$R), and (*d*) **helix 5**(D_2R)-**helix 4**(A_{2A}R). The second set of contacts includes: (*a*) **helix 3$_{C\text{-terminal half}}$**($D_2$R)-**helix 4$_{C\text{-terminal half}}$**-($A_{2A}$R), (*b*) **helix 4$_{N\text{-terminal half}}$**($D_2$R)-**helix 5$_{N\text{-terminal half}}$**-($A_{2A}$R), (*c*) **helix 5**($D_2$R)-**helix 4**($A_{2A}$R), and (*d*) **I3**(D2R)-**C-tail**(A_{2A}R) (only a few contacts).

DISCUSSION

Adenosine-dopamine interactions play a very important role in basal ganglia function and dysfunction. This is the result of the existence of specific antagonistic interactions between different adenosine and dopamine receptor subtypes co-localized in different neurons of the striatum, the main input structure of the basal ganglia. Two subtypes of GABAergic efferent neurons, the striatonigral and the striatopallidal neurons, constitute more than 90% of the striatal neuronal population. The interaction of A_1Rs and D_1Rs modulates the function of striatonigral neurons, whereas the interactions of A_{2A}R and D_2R modulates the function of striatopallidal neurons (5, 7, 8). The existence of functional A_1R-D_1R and A_{2A}R-D_2R heteromeric complexes has recently been demonstrated in mammalian cell lines (10, 27). However, the techniques used in previously reported data, including co-immunoprecipitation and confocal laser microscopy co-localization studies, could not discard the possibility of a third protein acting as scaffolding to bring the two receptors together.

In the present work, we have used FRET and BRET techniques to demonstrate that, in fact, A_{2A}R and D_2R form heteromers in living cells. This interaction was found to be specific where no BRET or FRET signals were detected when other receptors were assayed (see "Results"). The estimated distance between the fluorophores fused to C-terminal tails of A_{2A}R and D_2R resulted to be ~6.3 nm. Receptor molecules with very close proximity in small membrane microdomains can lead to artifactual BRET results, as with proteins targeted to cholesterol-rich plasma membrane domains by lipid anchoring clusters in rafts (23). This was ruled out by the unmodified BRET signal between A_{2A}R-*Rluc* and D_2R-YFP in the presence of cyclodex-

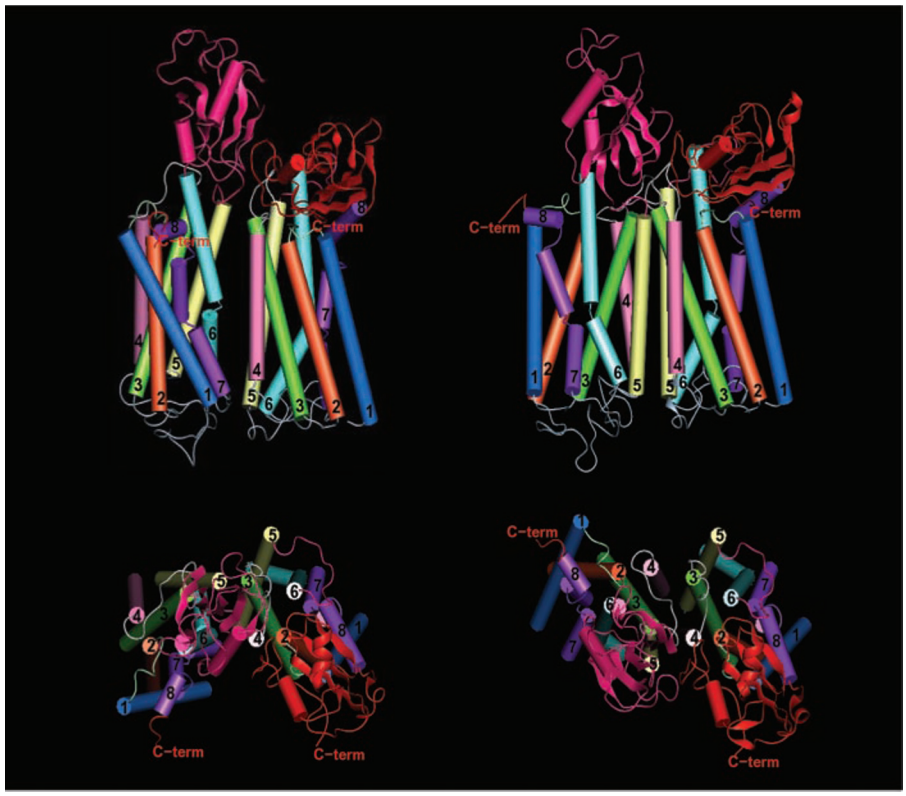

FIG. 10. **Examples of the D_2R-$A_{2A}R$ heterodimers belonging to population 1 (*top* and *bottom left*) and to population 2 (*top* and *bottom right*).** In the *top views*, the helix bundles are seen in a direction parallel to the membrane surface, the intracellular side being at the *top*. In the *bottom views*, the helix bundles are seen from the intracellular side in a direction almost perpendicular to the membrane surface. Helices 1, 2, 3, 4, 5, 6, and 7 are, respectively, *blue*, *orange*, *green*, *pink*, *yellow*, *cyan*, and *violet*. The amino acid stretch corresponding to helix 8 of rhodopsin is *violet* as well. The extracellular domains are *gray*, whereas the intracellular loops 1, 2 and 3 and the C-tail (*C-term*) are, respectively, *light green*, *white*, *purple*, and *red*.

trin, which disrupts rafts and prevents the eventual accumulation of receptors in these structures (Fig. 6).

Homomerization and heteromerization of GPCRs have been suggested to involve different receptor domains. The C-terminal tail of the GABA receptors is involved in $GABA_BR1$-$GABA_BR2$ heteromerization by a coiled-coil interaction (28, 29). X-ray studies performed with the metabotropic glutamate receptor $mGlu_1R$ have shown that its extracellular N-terminal ligand-binding region forms disulfide-linked homodimers (30). There is also evidence for the transmembrane domains in mediating the formation of homo- or heterodimers (for review, see Ref. 1). The sixth and seventh helices of D_2R have been implicated in its homodimerization, because synthesized peptides encoding sequences in these regions inhibit dimer formation (31). Furthermore, Guo *et al.* (32) have recently reported that D_2R homodimers are stabilized by cross-linking through a cysteine residue located at the extracellular end of helix 4. The present results using the previously characterized chimeric D_2R-D_1R containing helices 5 and 6, I3, and E3 of the dopamine D_1R (9), demonstrate that these portions of the D_2R are directly involved in the formation of $A_{2A}R$-D_2R heteromers. Thus, differing from the wild-type D_2R, the chimeric D_2R-D_1R was not able to compete for the specific BRET between $A_{2A}R$-*Rluc* and D_2R-YFP.

To gain insight into the potential D_2R-$A_{2A}R$ heterodimer interfaces, rigid-body docking simulations have been done between an average minimized structure of D_2R and nine different average minimized structures of $A_{2A}R$. From docking simulations two sets of dimers sharing (within each set) similar interdimer interfaces have been obtained (population 1 and population 2, see Fig. 10). In particular, in the most populated one (population 1), helix 5 and/or helix 6 and the N-terminal portion of I3 from D_2R approach helix 4 and the C-terminal portion of the C-tail from the $A_{2A}R$, respectively. Helix 7(D_2R) may also participate together with helix 6 in the contacts with helix 4($A_{2A}R$) (Fig. 10, *left side*). The interface contacts in population 1 are consistent with the results of BRET experiments done in this work on the chimeric D_2R-D_1R and $A_{2A}R$. Population 2 has a reduced number of structures if compared with population 1. However, structures in population 2 display high docking scores and resemble the intradimer contact model proposed for rhodopsin (26).

The analysis of the BRET signal in $A_{2A}R$-D_2R-expressing cells indicated that the activation of $A_{2A}R$ or D_2R by their corresponding agonist did not affect the degree of heteromerization. Similar results were obtained when the two agonists were used simultaneously (Fig. 7). The lack of modulation by agonists has also been reported for other homo- and heterodimeric partners (3, 33, 34). In carefully controlled BRET studies, it has been demonstrated that a number of heteromerizing receptors are pre-assembled in the ER and the dimers that reach the plasma membrane are not affected, in terms of the degree of dimerization, after receptor activation by their corresponding ligands (33–36). In contrast to this recently reported data, detailed studies by Patel *et al.* (37) in stable CHO-K1 cells expressing somatostatin receptors suggest that the receptors are monomeric in their basal state and oligomerize only upon agonist activation. For the somatostatin receptor subtype R5, the same authors report that ligand-induced homomerization extends beyond dimers to higher order oligomers (39). For our experimental data, the unchanged BRET signal reported in cells treated with agonists is not necessarily in contradiction to the known clustering of these receptors when they are activated by agonists. In fact, the $A_{2A}R$ agonist CGS21680 leads to the clustering of $A_{2A}R$ receptors in neuroblastoma SH-SY5Y cells or in primary neuronal cell cultures, and similar clustering occurs with D_2R receptors when D_2R-expressing cells are treated with the D_2R agonist quinpirole (10). It should also be noted that co-clustering of $A_{2A}R$ and D_2R occurs when either agonist is added, alone or simultaneously, to cells co-expressing both receptors (10). Taken together these results indicate that $A_{2A}R$ or D_2R agonists lead to the reorganization of receptors within the plasma membrane while not affecting their degree of heterodimerization. Considering the

data, it appears as if ligand-induced activation of the receptors leads to target pre-existing $A_{2A}R$-D_2R heterodimers to membrane microdomains. Ligand modulation of heteromers may also be dependent upon the nature of the receptors involved and their level of expression. It should not be ruled out that other factors might also contribute to this modulation. Further research is required to understand whether ligand regulation is dependent on the particular expression of scaffold or chaperone proteins in cell models where ligand modulation of receptor oligomerization is studied.

Receptor-receptor heteromerization serves a variety of purposes in receptor function. For instance, assembly of heterodimers is required for targeting $GABA_B$ receptors to the cell surface (38). $GABA_BR1$-$GABA_BR2$ heterodimerization is necessary for $GABA_B$ receptor signaling, because one of the receptors within the heterodimer binds the ligand whereas the other is linked to the signaling machinery. Moreover, $GABA_BR2$ is required to provide high affinity for agonists to the $GABA_BR1$ subunit (39). We have previously postulated that heterodimerization may be necessary for intramembrane receptor-receptor interactions, where the stimulation of one receptor changes the binding characteristics of another receptor in tissue or cell membrane preparations (5, 40–42). An intramembrane $A_{2A}R$-D_2R antagonistic interaction has been repeatedly demonstrated in both rat and human striatum as well as in transfected mammalian cell lines, where the stimulation of $A_{2A}R$ decreases the affinity of D_2R receptor for agonists (9, 43–47). In CHO-transfected cells, the $A_{2A}R$ agonist CGS 21680 decreased the affinity of the D_2R but not of the chimeric D_2R-D_1R for tritiated dopamine (25). Taken together with the above-mentioned results, this strongly suggests that the intramembrane $A_{2A}R$-D_2R interaction depends on the heteromerization between $A_{2A}R$ and D_2R. It is very probable that the loss of affinity to dopamine binding of the D_2R when the $A_{2A}R$ is activated is a result of conformational changes transmitted through the heteromeric interaction. Interestingly, there is an increase in the agonist binding affinity for D_2R with an enhancement of G protein and effector coupling to adenylyl cyclase when the D_2R and somatostatin SSTR5 receptors heteromerize in response to agonist treatment (48). Therefore, the increase or decrease in the affinity of agonist binding to D_2R would depend on the nature of the heteromeric partner; SSTR5 receptors leading to an increase in its affinity (*i.e.* synergy) and $A_{2A}R$ leading to a decrease (*i.e.* antagonism). This and other potential roles of the $A_{2A}R$-D_2R heteromers are important to fully understand the molecular basis of the adenosine-dopamine antagonism within the central nervous system, thus allowing for the design of novel strategies to combat basal ganglia disorders (like Parkinson's disease), schizophrenia, and drug addiction.

REFERENCES

1. Bouvier, M. (2001) *Nat. Rev. Neurosci.* **2,** 274–286
2. Milligan, G., and White, J. H. (2001) *Trends Pharmacol. Sci.* **22,** 513–518
3. Rios, C. D., Jordan, B. A., Gomes, I., and Devi, L. A. (2001) *Pharmacol. Ther.* **92,** 71–87
4. George, S. R., O'Dowd, B. F., and Lee, S. P. (2002) *Nat. Rev. Drug Discov.* **1,** 808–820
5. Agnati, L. F., Ferré, S., Lluis, C., Franco, R., and Fuxe, K. (2003) *Pharmacol. Rev.* **55,** 509–550
6. Franco, R., Canals, M., Marcellino, D., Ferré, S., Agnati, L. F., Mallol, J., Casadó, V., Ciruela, F., Fuxe, K., Lluis, C., and Canela, E. I. (2003) *Trends Biochem. Sci.* **28,** 238–243
7. Ferré, S., Fredholm, B. B., Morelli, M., Popoli, P., and Fuxe, K. (1997) *Trends Neurosci.* **20,** 482–487
8. Ferré, S., Ciruela, F., Woods, A. S., Canals, M., Burgueno, J., Marcellino, D., Karcz-Kubicha, M., Hope, B. T., Morales, M., Popoli, P., Goldberg, S. R., Fuxe, K., Lluis, C., Franco, R., and Agnati, L. F. (2003) *Curr. Med. Chem.* **3,** 1–26
9. Ferré, S., von Euler, G., Johansson, B., Fredholm, B. B., and Fuxe, K. (1991) *Proc. Natl. Acad. Sci. U. S. A.* **88,** 7238–7241
10. Hillion, J., Canals, M., Torvinen, M., Casado, V., Scott, R., Terasmaa, A., Hansson, A., Watson, S., Olah, M. E., Mallol, J., Canela, E. I., Zoli, M., Agnati, L. F., Ibanez, C. F., Lluis, C., Franco, R., Ferré, S., and Fuxe, K. (2002) *J. Biol. Chem.* **277,** 18091–18097
11. Kozell, L. B., and Neve, K. A. (1997) *Mol. Pharmacol.* **52,** 1137–1149
12. Zimmermann, T., Rietdorf, J., Girod, A., Georget, V., and Pepperkok, R. (2002) *FEBS Lett.* **531,** 245–249
13. Jordan, M., Schallhorn, A., and Wurm, F. M. (1996) *Nucleic Acids Res.* **24,** 596–601
14. Sali, A., and Blundell, T. L. (1993) *J. Mol. Biol.* **234,** 779–815
15. Jones, D. T., Taylor, W. R., and Thornton, J. M. (1992) *Nature* **358,** 86–89
16. Palczewski, K., Kumasaka, T., Hori, T., Behnke, C. A., Motoshima, H., Fox, B. A., Le Trong, I., Teller, D. C., Okada, T., Stenkamp, R. E., Yamamoto, M., and Miyano, M. (2000) *Science* **289,** 739–745
17. Brooks, B. R., Bruccoleri, R. E., Olafson, B. D., States, D. J., Swaminathan, S., and. Karplus, M. (1983) *J. Comput. Chem.* **4,** 187–217
18. Ballesteros, J. A., and Weinstein, H. (1995) *Methods Neurosci.* **25,** 366–428
19. Chen, R., Li L., and Weng, Z. (2003) *Proteins* **52,** 80–87
20. Ausiello, G., Cesareni, G., and Helmer-Citterich, M. (1997) *Proteins* **28,** 556–567
21. Angers, S., Salahpour, A., and Bouvier, M. (2002) *Annu. Rev. Pharmacol. Toxicol.* **42,** 409–435
22. Mercier, J. F., Salahpour, A., Angers, S., Breit, A., and Bouvier, M. (2002) *J. Biol. Chem.* **277,** 44925–44931
23. Zacharias, D. A., Violin, J. D., Newton, A. C., and Tsien, R. Y. (2002) *Science* **296,** 913–916
24. Furuchi, T., and Anderson, R. G. (1998) *J. Biol. Chem.* **273,** 21099–21104
25. Torvinen, M., Liu, Y., Kozell, L. B., Neve, K. A., Ferré, S., Ibañez, C., and Fuxe, K. (2001) *Soc. Neurosci. Abstr.* **27,** 379
26. Liang, Y., Fotiadis, D., Filipek, S., Saperstein, D. A., Palczewski, K., and Engel, A. (2003) *J. Biol. Chem.* **278,** 21655–21662
27. Ginés, S., Hillion, J., Torvinen, M., Le Crom, S., Casado, V., Canela, E. I., Rondin, S., Lew, J. Y., Watson, S., Zoli, M., Agnati, L. F., Vernier, P., Lluis, C., Ferré, S., Fuxe, K., and Franco, R. (2000) *Proc. Natl. Acad. Sci. U. S. A.* **97,** 8606–8611
28. Kuner, R., Kohr, G., Grunewald, S., Eisenhardt, G., Bach, A., and Kornau, H. C., (1999) *Science* **283,** 74–77
29. Kammerer, R. A., Frank, S., Schulthess, T., Landwehr, R., Lustig, A., and Engel, J. (1999) *Biochemistry* **38,** 13263–13269
30. Kunishima, N., Shimada, Y., Tsuji, Y., Sato, T., Yamamoto, M., Kumasaka, T., Nakanishi, S., Jingami, H., and Morikawa, K. (2000) *Nature* **407,** 971–977
31. Ng, G. Y., O'Dowd, B. F., Lee, S. P., Chung, H. T., Brann, M. R., Seeman, P., and George, S. R. (1996) *Biochem. Biophys. Res. Commun.* **227,** 200–204
32. Guo, W., Shi, L., and Javitch, J. A. (2003) *J. Biol. Chem.* **278,** 4385–4388
33. Issafras, H., Angers, S., Bulenger, S., Blanpain, C., Parmentier, M., Labbe-Jullie, C., Bouvier, M., and Marullo, S. (2002) *J. Biol. Chem.* **277,** 34666–34673
34. Terrillon, S., Durroux, T., Mouillac, B., Breit, A., Ayoub, M. A., Taulan, M., Jockers, R., Barberis, C., and Bouvier, M. (2003) *Mol. Endocrinol.* **17,** 677–691
35. Jensen, A. A., Hansen, J. L., Sheikh, S. P., and Brauner-Osborne, H. (2002) *Eur. J. Biochem.* **269,** 5076–5087
36. Ramsay, D., Kellet, E., McVey, M., Rees, S., and Milligan, G. (2002) *Biochem. J.* **365,** 429–440
37. Patel, R. C., Kumar, U., Lamb, D. C., Eid, J. S., Rocheville, M., Grant, M., Rani, A., Hazlett, T., Patel, S. C., Gratton, E., and Patel, Y. C. (2002) *Proc. Natl. Acad. Sci. U. S. A.* **99,** 3294–3299
38. White, J. H., Wise, A., Main, M. J., Green, A., Fraser, N. J., Disney, G. H., Barnes, A. A., Emson, P., Foord, S. M., and Marshall, F. H. (1998) *Nature* **396,** 679–682
39. Kniazeff, J., Galvez, T., Labesse, G., and Pin, J. P. (2002) *J. Neurosci.* **22,** 7352–7361
40. Agnati, L. F., Fuxe K., Zini I., Lenzi P., and Hökfelt T. (1980) *Med. Biol.* **58,** 182–187
41. Fuxe, K., and Agnati, L. F. (1985) *Med. Res. Rev.* **5,** 441–482
42. Zoli, M., Agnati, L. F., Hedlund, P. B., Li, X.-M., Ferré, S., and Fuxe, K. (1993) *Mol. Neurobiol.* **7,** 293–334
43. Dasgupta, S., Ferré, S., Kull, B., Hedlund, P. B., Finnman, U. B., Ahlberg, S., Arenas, E., Fredholm, B. B., and Fuxe, K. (1996) *Eur. J. Pharmacol.* **316,** 325–331
44. Dixon, A. K., Widdowson, L., and Richardson, P. J. (1997) *J. Neurochem.* **69,** 315–321
45. Kull, B., Ferré, S., Arslan, G., Svenningsson, P., Fuxe, K., Owman, C., and Fredholm, B. B. (1999) *Biochem. Pharmacol.* **58,** 1035–1045
46. Salim, H, Ferré, S., Dalal, A., Peterfreund, R. A., Fuxe, K., Vincent, J. D., and Lledo, P. M. (2000) *J. Neurochem.* **74,** 432–439
47. Díaz-Cabiale, Z., Hurd, Y., Guidolin, D., Finnman, U.-B., Zoli, M., Agnati, L. F., Vanderhaeghen, J.-J., Fuxe, K., and Ferré, S. (2001) *Neuroreport* **12,** 1831–1834
48. Rocheville, M., Lange, D. C., Kumar, U., Patel, S. C., Patel, R. C., and Patel, Y. C. (2000) *Science* **288,** 154–157